Altitudinal Gradients of Stable Isotopes in Lee-Slope Precipitation in the Canadian Rocky Mountains

Authors: Moran, Tara A., Marshall, Shawn J., Evans, Erin C., and Sinclair, Kate E.

Source: Arctic, Antarctic, and Alpine Research, 39(3) : 455-467

Published By: Institute of Arctic and Alpine Research (INSTAAR), University of Colorado

URL: https://doi.org/10.1657/1523-0430(06-022)[MORAN]2.0.CO;2

Arctic, Antarctic and Alpine Research, Vol. 39, No. 3, 2007, pp. 455–467

Altitudinal Gradients of Stable Isotopes in Lee-Slope Precipitation in the Canadian Rocky Mountains

*Tara A. Moran**§*
*Shawn J. Marshall**†*
Erin C. Evans‡ and
*Kate E. Sinclair**

*Department of Geography, University of Calgary, Calgary, AB, T2N 1N4, Canada
†W. Garfield Weston Foundation Fellow, Canadian Institute for Advanced Research, 180 Dundas Street West, Suite 1400, Toronto, ON, M5G 1Z8, Canada
‡Department of Atmospheric and Oceanic Sciences, McGill University, Montreal, QC, H3A 2K6, Canada
§Corresponding author.
tamoran@ucalgary.ca

Abstract

Fresh snow samples were collected following seven snow accumulation events along an altitudinal transect of the Robertson Valley. This glacierized valley is on the eastern slopes of the Canadian Rockies at the Continental Divide and receives precipitation from both westerly (Pacific) air masses and from easterly (upslope) systems. Snow samples were collected over two winter seasons and were analyzed for $\delta^{18}O$, revealing altitudinal gradients that ranged from −0.3‰/100 m to +1.8‰/100 m. Five of seven snow events had positive (inverse) isotopic gradients with altitude: ^{18}O enrichment at higher altitudes. Surface and upper-air meteorological data were analyzed to classify the type of weather systems bringing precipitation to the area for each accumulation event. Three storm classifications were developed: westerly, upslope, and mixed/northwesterly systems. Positive $\delta^{18}O$-elevation gradients were found under strong westerly and northwesterly flow, when the Robertson Valley acts as a leeward slope, while more conventional negative gradients correspond with upslope flow, when easterly winds make the Robertson Valley a windward snow deposition environment. We interpret the inverse isotopic gradients as evidence of ongoing Rayleigh distillation as westerly systems cross the Continental Divide. Position on the Rayleigh distillation curve had a strong influence on the magnitude of $\delta^{18}O$-elevation gradients.

DOI: 10.1657/1523-0430(06-022)[MORAN]2.0.CO;2

Introduction

The general effects of altitude, latitude, and continentality on stable isotopes in precipitation (^{18}O, D) were established by Craig (1961) and Dansgaard (1964) and have been broadly confirmed by the long-term sampling program of the Global Network of Isotopes in Precipitation (IAEA/WMO, 2004). Condensation of water vapor in an air mass favors heavy isotopes, leaving isotopically depleted vapor in the residual air mass. Since condensation and rainout result from cooling of air masses, this isotopic fractionation and distillation can be driven by vapor transport to higher altitudes, higher latitudes, or interior continental regions. Cooling or humidification can also result from mixing of air masses. In reality, mid-latitude precipitation is commonly generated by a combination of these cooling mechanisms. The general result is that precipitation becomes progressively depleted in heavy isotopes as a function of increasing latitude, altitude, or distance from the coast.

The altitudinal decrease in heavy isotopes has been observed on windward slopes throughout the globe, as measured by the ratio of either ^{18}O to ^{16}O ($\delta^{18}O$) or D to H (δD) in precipitation samples (e.g., Gat, 1980; Różański et al., 1993). Orographic uplift and adiabatic cooling of air masses lead to saturation, condensation, and rainout, with fractionation during condensation leading to isotopically depleted precipitation at higher elevations. Altitudinal gradients of $\delta^{18}O$ generally range from −0.1‰/100 m to −0.6‰/100 m for a global distribution of sites (Ambach et al., 1968; Friedman and Smith, 1970; Moser and Stichler, 1974; Gat et al., 2000: 55), although gradients exceeding −1.0‰/100 m have been measured in polar regions (Dansgaard et al., 1973; Lorius and Merlivat, 1975). These gradients are of interest because they are used to reconstruct altitude in a variety of geological, hydrological, and paleoclimatological applications. For instance, global or regional $\delta^{18}O$ lapse rates are adopted in reconstructions of mountain uplift history or paleotopography from the ^{18}O content of authigenic or pedogenic clay minerals (Drummond et al., 1993; Chamberlain and Poage, 2000; Garzione et al., 2000; Dettman and Lohmann, 2000; Bowen and Wilkinson, 2002; Rowley and Currie, 2006). Pierrehumbert (1999) uses a model of vapor transport and isotope fractionation, along with reconstructions of vertical gradients in stable isotopes, to infer past climate conditions in the Andes. Stable isotopes in bulk water samples from rivers, lakes, springs, or groundwater systems are also used to assess the provenance of water in hydrological systems (Grasby and Lepitzki, 2002; Gat et al., 2000: 53). This requires assumptions about altitudinal gradients in $\delta^{18}O$ or δD in mountain catchments.

Variations in the altitudinal gradient of $\delta^{18}O$ and δD reflect differences in the vapor content and thermodynamic history of an air mass (e.g., Rowley et al., 2001). The isotopic evolution of water vapor during condensation and rainout from an idealized air mass is commonly modeled as a Rayleigh distillation process (Fig. 1),

$$R_v(f) = R_{v0} f^{[\alpha_{l-v}(T) - 1]}, \quad (1)$$

where R_{v0} is the initial isotopic ratio in the vapor mass (e.g., $^{18}O/^{16}O$), R_v is the isotopic ratio when only a fraction (f) of the vapor remains, and α_{l-v} (T) is the equilibrium fractionation factor for evaporation, which is a function of temperature, T. Rayleigh distillation assumes that the product of the reaction (vapor in evaporation processes or condensate during rainout) is immediately removed from the system. In the scenario of Figure 1, liquid condensate rains out of the air mass with an isotope ratio $\delta^{18}O_l$, calculated from

$$\delta^{18}O_l = \alpha_{l-v}\left(\delta^{18}O_v + 1000\right) - 1000. \quad (2)$$

1523-0430/07 $7.00

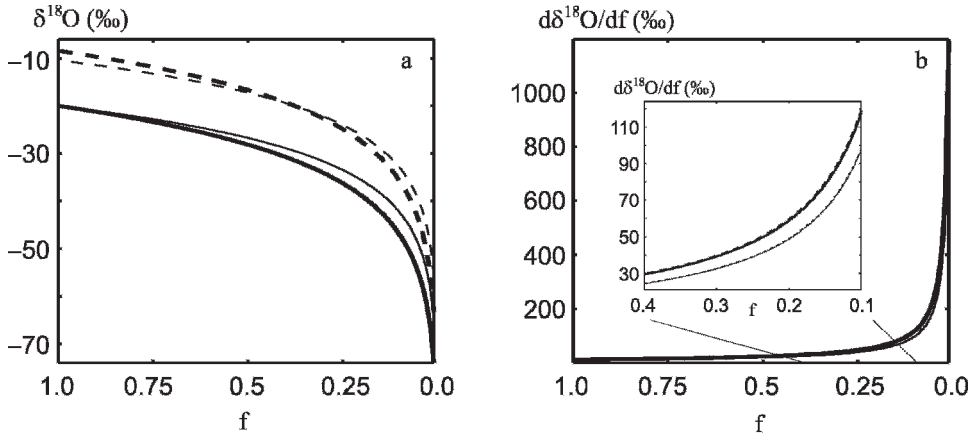

FIGURE 1. Rayleigh distillation of ^{18}O for equilibrium condensation of vapor at 0°C (heavy lines) and 20°C (thin lines). Solid lines are for the cloud vapor and dashed lines are for the condensate. The vapor is assigned an initial isotopic ratio, $\delta^{18}O_{v0}$, of −20‰ ($f = 1$), where f is the fraction of initial vapor remaining in the cloud. (a) Evolution of $\delta^{18}O$ in the vapor and condensate during rainout. (b) The rate of change of $\delta^{18}O$ with f, illustrating the non-linear depletion in $\delta^{18}O$ along the trajectory of a precipitating air mass undergoing Rayleigh-governed condensation and rainout.

The curves in Figure 1 depict isothermal Rayleigh distillation at temperatures of 20°C (thin lines) and 0°C (heavy lines) for an air parcel with an initial isotopic ratio of $\delta^{18}O_0 = -20‰$. Dashed lines in Figure 1 depict $\delta^{18}O_l$ and solid lines depict the isotopic evolution of vapor in the air mass, $\delta^{18}O_v$. Following Pierrehumbert (1999), equilibrium fractionation coefficients are calculated from the experimentally derived relationships of Horita et al. (1994) and Majoube (1971),

$$1000 \ln[\alpha(T)_{l-v}] = -7.685 + 6.7123 \times 10^3 T^{-1} - 1.6664 \times 10^6 T^{-2} + 0.35041 \times 10^9 T^{-3}. \quad (3)$$

Figure 1b plots $d\delta^{18}O/df$ for the idealized case of isothermal distillation, with the inset enlarging the zone $f \in [0.1, 0.4]$. As is clear in the plots, the late stages of rainout ($f \rightarrow 0$) are associated with rapid decreases in $\delta^{18}O_l$ and $\delta^{18}O_v$. The *rate* of decrease in $\delta^{18}O$ also increases exponentially as the air mass dries out, and is greater at cooler temperatures. From these plots, it is clear that isotopic gradients in precipitation samples along the trajectory of an air mass will vary depending on both temperature and the position on the Rayleigh distillation curve. Steeper gradients should be expected as the moisture content of the air mass becomes depleted, as often occurs at high elevations and at extremely continental sites.

In this paper, we investigate the isotope-elevation relationship in a lee-slope environment in the Canadian Rockies, a meteorological situation that is more complex than upslope, orographically induced rainout. Poage and Chamberlain (2001) provide a compilation of observed $\delta^{18}O$-elevation gradients from 68 different studies worldwide, with all but two of these sites reporting $\delta^{18}O$ depletion with altitude. Ambiguous or inverse $\delta^{18}O$-elevation relationships have been reported from eastern (lee) slope settings in the Sierra Nevada (Friedman and Smith, 1970) and the Canadian Rockies (Grasby and Lepitski, 2002). Complex altitudinal relationships are also evident in high alpine snow samples (> 5000 m altitude) from the central Hindu Kush, Afghanistan (Niewodniczański et al., 1981), the St. Elias Mountains, Canada (Holdsworth et al., 1991), and possibly at high altitudes on Mt. Blanc, France (Moser and Stichler, 1974). This disruption of typical $\delta^{18}O$-elevation gradients has been attributed to post-depositional modification, secondary moisture sources, or turbulent mixing of air masses on the lee side of topographic barriers.

The $\delta^{18}O$-elevation relationship in lee-slope environments will reflect the mechanisms of moisture transport and deposition. If precipitation results from continued rainout of air masses as they traverse topographic barriers, then continued Rayleigh distillation on the lee slope should indeed produce an inverse relationship with altitude—lighter isotopic ratios with decreasing altitude. This would suggest a systematic altitudinal relationship that is the opposite of that which is observed on windward slopes, but an inverse relationship of this type is not well established or widely reported. Part of the complication may arise from turbulent mixing of air masses as they are forced up and over topographic barriers; isotopic signatures on lee slopes will depend on the temperature and moisture content of mid-troposphere or lee-side air masses that are entrained. In addition, the question is likely to be scale and season dependent. Snow falling from clouds is typically swept downwind, with horizontal displacements of up to tens of kilometers (Banta, 1990; Roe, 2005). Since condensation in this situation is driven by moist adiabatic cooling during upslope, orographic ascent, lee-slope deposition will reflect continued Rayleigh distillation well downstream of the topographic barrier, independent of the lee-side terrain. The effect would be less pronounced with rainfall, which experiences less downwind drift, and with air masses/precipitating systems that are near the surface.

Finally, areas like the eastern slopes of the Canadian Rocky Mountains are susceptible to easterly, upslope storms that act as classical orographic systems (Stewart et al., 1995). If precipitation in the eastern slopes is dominated by these weather systems, more standard $\delta^{18}O$-elevation relationships (depletion with altitude) would prevail. Upslope storms of this type are common in the Canadian Rockies in spring, when cyclonic disturbances commonly track through the region to the south and east and are intensified by orographically enhanced upper-level divergence (Chung et al., 1976; Stewart et al., 1995). The extent of winter-season and total annual moisture transport to the eastern slopes of the Rockies from upslope systems is unknown. Because of these competing meteorological processes and their distinct isotopic behavior, we hypothesize that the isotopic character of precipitation samples from the eastern slopes can provide insight into the synoptic weather systems that govern precipitation in the region. This would be valuable because the complete winter snowpack stratigraphy could then be interpreted in terms of weather systems that dictate seasonal moisture supply, offering a new tool for water resource forecasts and glacier mass-balance studies.

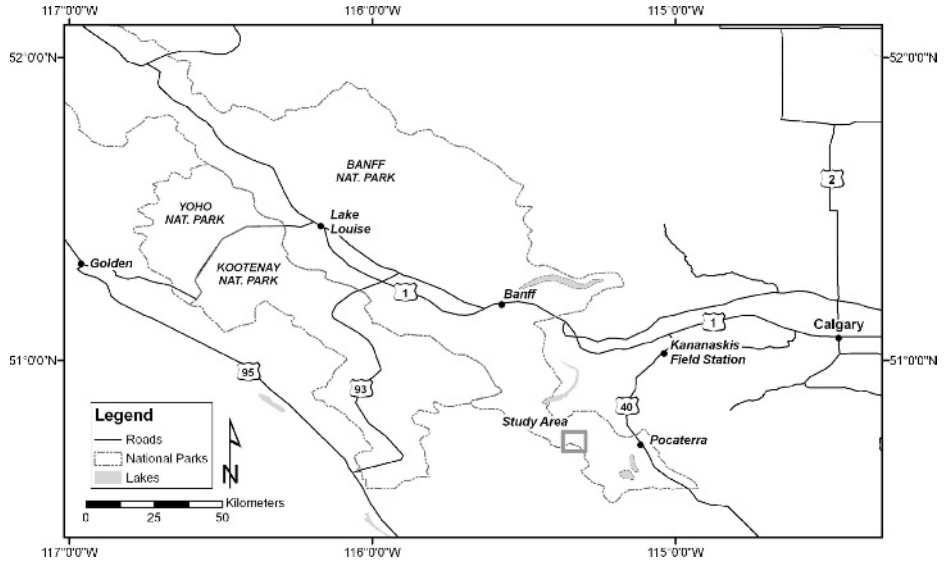

FIGURE 2. Location of the study site and nearby Meteorological Service of Canada weather records used in the interpretation of snow accumulation events.

Study Site and Methods

We are testing this hypothesis in the Robertson Valley (50.7°N, 115.3°W), which is situated on the eastern slopes of the Canadian Rocky Mountains, 102 km southeast of Calgary, Alberta (Fig. 2). It is a steep, glacierized alpine valley 6 km long, with the Robertson Glacier occupying the upper 2.8 km of the valley (Fig. 3). The head of the glacier is positioned at a col at an elevation of approximately 2950 m a.s.l., which also marks the North American Continental Divide (Robs10 in Fig. 3). The glacier terminus is at an altitude of 2370 m (Robs04 in Fig. 3) and the lower Robertson Valley is at 1980 m (site Robs02 in Fig. 3). The hydrology of the area is dominated by springtime meltwater that feeds into the Spray River and subsequently to the Bow River, the major mountain drainage system in southern Alberta. Understanding storm systems that bring wintertime precipitation into the area and the amount of precipitation from different weather systems will become increasingly important as stress on southern Alberta's water resources grows (e.g., Byrne et al., 1999; Rood et al., 2005; Barnett et al., 2005).

From 2002 to 2004 we analyzed $\delta^{18}O$ vs. altitude in fresh snow samples from seven separate winter storms in the Robertson Valley. We confined our study to significant, regional-scale precipitation events in which the beginning and end of the snowfall could be clearly identified in meteorological records and total snow accumulation was sufficient to permit unequivocal sampling of the fresh snow deposit. Snow samples were collected as soon as possible following each precipitation event, typically with a delay of several days due to high avalanche hazard immediately following a major snowfall in the region (Table 1). In one case, we did not get into the site until 17 days after the snow event. Post-depositional modification of *in situ* snow isotopes is negligible as long as temperatures remain below freezing between the time of deposition and the time when they are sampled. Once snow has experienced partial melt, however, evaporation of the lighter isotopes can leave the snowpack isotopically enriched (Niewodniczański et al., 1981). In order to avoid potential problems associated with post-depositional modification, accumulation events were not sampled if air temperatures reached 0°C before we could sample the snow. In the absence of melt, the depositional archive may still be modified by wind scour and wind-driven redistribution of snow (Holdsworth et al., 1991). We were unable to control for this, and wind effects may taint some high elevation samples where downglacier winds are strong and persistent.

For each of the seven snow accumulation events, snow samples were collected from the nine sites in the Robertson Glacier and Valley along with an additional sample from the Burstall Pass trailhead (Robs01, 1900 m a.s.l.), where we gain access to the area (Fig. 3 and Table 1). Grab samples of fresh snow were taken at roughly 100 m intervals, as determined by a handheld GPS. Surface snow was brushed away from each sample site to minimize the effects of wind redistribution and potential surface sublimation/deposition, and a bulk sample of the underlying fresh snow deposit was collected in a plastic freezer bag for transport to the stable isotope laboratory at the University of Calgary. Samples were then thawed at room temperature and bottled in 20 ml glass sample vials, which were then capped, sealed with Parafilm, and refrigerated upside down to prevent evaporation until samples were analyzed. Weather and travel conditions prohibited a complete sample collection for the final storm in the dataset, and samples are missing from earlier storm samples due to human error (puncture and leakage of the sample or missing a site during the sampling due to poor GPS reception). In the isotope lab, water samples were equilibrated with CO_2 gas, which was then pumped into a dual-inlet isotope ratio mass spectrometer (IRMS) to determine the $^{18}O/^{16}O$ ratio. The uncertainty of $\delta^{18}O$ measurement is $\pm$ 0.2‰.

Seven of the ten sampling sites were equipped with temperature-humidity dataloggers, recording at 30 minute intervals through winter 2003–2004 (Table 2). An automatic weather station (AWS) from the neighboring Haig Glacier (see Fig. 3) recorded temperature, relative humidity, atmospheric pressure, wind speed and direction, solar radiation, and snow accumulation at 30 minute intervals, with snow depth measured by an ultrasonic depth gauge.

Results

$\delta^{18}O$-ELEVATION GRADIENTS

$\delta^{18}O$ was regressed as a function of elevation for each of the snow accumulation events. As summarized in Table 3, $\delta^{18}O$-elevation gradients ranged from −0.3‰/100 m to +1.8‰/100 m in the seven storms. The raw data and regressions are shown in Figure 4. There is considerable scatter in the data, but a statisti-

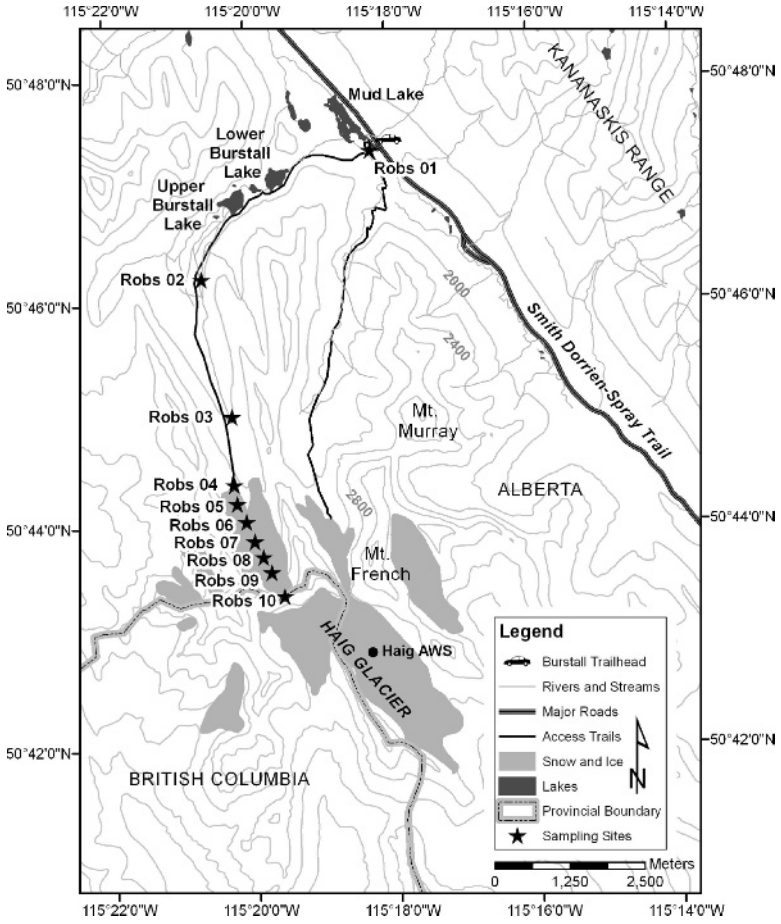

FIGURE 3. Snow sampling site locations (indicated by stars) on the Robertson Glacier and in the Burstall Valley, Peter Lougheed Provincial Park, Alberta, Canada. The automated weather station on the neighboring Haig Glacier is indicated by a circle.

cally significant linear correlation was found in five of the seven snow events. The δ^{18}O-elevation gradients observed in the Robertson Valley differ markedly from the average altitudinal gradients observed on the windward slope of storm tracks, which have values of −0.5‰/100 m to −1.1‰/100 m, as discussed in the introduction. Five of the seven storm systems that we sampled produced inverse (positive) isotopic gradients—greater ^{18}O depletion at low altitudes. One storm exhibited no significant altitudinal trend, and one storm aligns with the normally reported negative altitudinal gradients.

Note that there was a data outlier associated with accumulation event 5. This storm was a low-accumulation event (approximately 4 cm) and was sampled four days after the end of the storm. As a result, the area may have been sensitive to wind redistribution, or we may have sampled the snowpack at too great of a depth (penetrating into a previous snow accumulation event). Calculations of isotopic gradients for accumulation event 5 included in Table 3 (+1.8‰/100 m with $p = 0.001$) omit the data outlier. The δ^{18}O-elevation gradient prior to the omission was +1.1‰/100 m, with $p = 0.14$ (not statistically significant).

METEOROLOGICAL ANALYSIS

Accumulation events were analyzed to determine storm origin and mechanisms in an attempt to explain the δ^{18}O-elevation gradients. Wintertime precipitation over the Canadian Rocky Mountains is controlled by orographic or convergent synoptic systems of two major air masses, maritime Pacific (mP) and continental Polar (cP) (Lapp et al., 2002). The influence of these air masses results in three main snow accumulation classifications for the seven snow accumulation events in this study: 1) westerly (zonal) storm systems, 2) easterly, upslope storms, and 3) northwesterly storm systems associated with a strong upper-level trough. These storm types are discussed in greater detail below.

TABLE 1

Snow accumulation events and sampling dates.

Sampling events	Snow accumulation dates	Sample date
1	February 10–11, 2002	February 15, 2002
2	March 15–16, 2002	March 17, 2002
3	October 28–30, 2003	November 7, 2003
4	November 10–11, 2003	November 14, 2003
5	January 1–3, 2004	January 7, 2004
6	January 23–31, 2004	February 17, 2004
7	February 27–March 7, 2004	March 7, 2004

TABLE 2

Sampling sites along the Robertson transect.

Site	Elevation (m)	Temperature-humidity datalogger
Robs 01	1905	Yes
Robs 02	1978	Yes
Robs 03	2073	Yes
Robs 04	2179	Yes
Robs 05	2438	Yes
Robs 06	2407	No
Robs 07	2510	Yes
Robs 08	2566	No
Robs 09	2735	No
Robs 10	2896	Yes

TABLE 3

$\delta^{18}O$-elevation gradients in the seven snow events.

Accumulation event	Gradient (‰/100 m)	Standard error	Adjusted R^2	Probability	Sample number (n)
1	0.5*	1.8	0.46	0.026	9
2	−0.3*	1.4	0.32	0.082	8
3	1.6*	3.8	0.66	0.003	10
4	0.7*	1.3	0.78	0.002	8
5	1.8*	3.1	0.18	0.001	8
6	0.3	2.3	0.08	0.255	8
7	−0.02	3.6	0.31	0.925	5

* Gradients significant at the 90% confidence level.

Though all seven of the snow accumulation events were placed into one of the three storm classifications, based on weather conditions when the bulk of precipitation fell, it should be noted that there was considerable within-storm variability.

Local weather data used for storm classification included: AWS data from the Haig Glacier; 30 minute temperature and relative humidity data from the Robertson Valley transect; hourly weather data from several Environment Canada monitoring sites in the region (Table 4) acquired from the Environment Canada data archive Web site at http://climate.weatheroffice.ec.gc.ca; and 700 mb water vapor mixing ratios from radiosonde data at the Kelowna International Airport, British Columbia (YLW). The nearest available upwind upper-air data was acquired from the University of Wisconsin, Department of Atmospheric Sciences Web site at http://weather.uwyo.edu/upperair/sounding.html. Additional synoptic data used for storm classification included reanalyzed daily 500 mb height maps and 850 and 700 mb vapor mixing ratios from the National Centre for Environmental Prediction (NCEP). NCEP Reanalysis data was acquired from the NOAA-CIRES ESRL/PSD Climate Diagnostics branch, Boulder, Colorado, U.S.A., from their Web site at http://www.cdc.noaa.gov/. Key weather parameters that form the basis of our storm classification are summarized in Table 5. NCEP pressure maps and surface weather charts played an important role in identifying the vapor mass origin and trajectory to the study area.

TABLE 4

Environment Canada and University of Calgary meteorological data sites used in the storm analysis. See Figures 2 and 3 for site locations.

Site	Latitude (°N)	Longitude (°W)	Elevation (m)	Description
Calgary Airport	51°06′	114°01′	1084	Eastern edge of foothills
Pocaterra	50°42′	115°07′	1610	Front ranges
Haig Glacier AWS	50°71′	115°30′	2674	Continental Divide
Golden, B.C.	51°18′	116°58′	785	Western slopes

Our meteorological and snow-course observations from the Robertson Valley indicate that the Haig Glacier meteorological records, within 2 km of the Robertson Glacier snow samples, are most representative of both temperature and snowfall in the Robertson Valley. We therefore use the Haig Glacier AWS as the primary determinant of start and end times for each snowfall event. In some events, it was clear that precipitation was sweeping across the region from west to east, with delays of up to one day between Golden and Calgary. In these cases, we extended the start or end time by one day to include the snowfall accumulations that led or lagged at nearby sites.

Westerly Storm Systems

Westerly flow predominates in the region, bringing large quantities of Pacific moisture to southern British Columbia (B.C.). These westerly systems traverse several mountain ranges in southern B.C., with altitudes ranging from 1500 to 3500 m. Altitudes generally increase eastward to the Continental Divide,

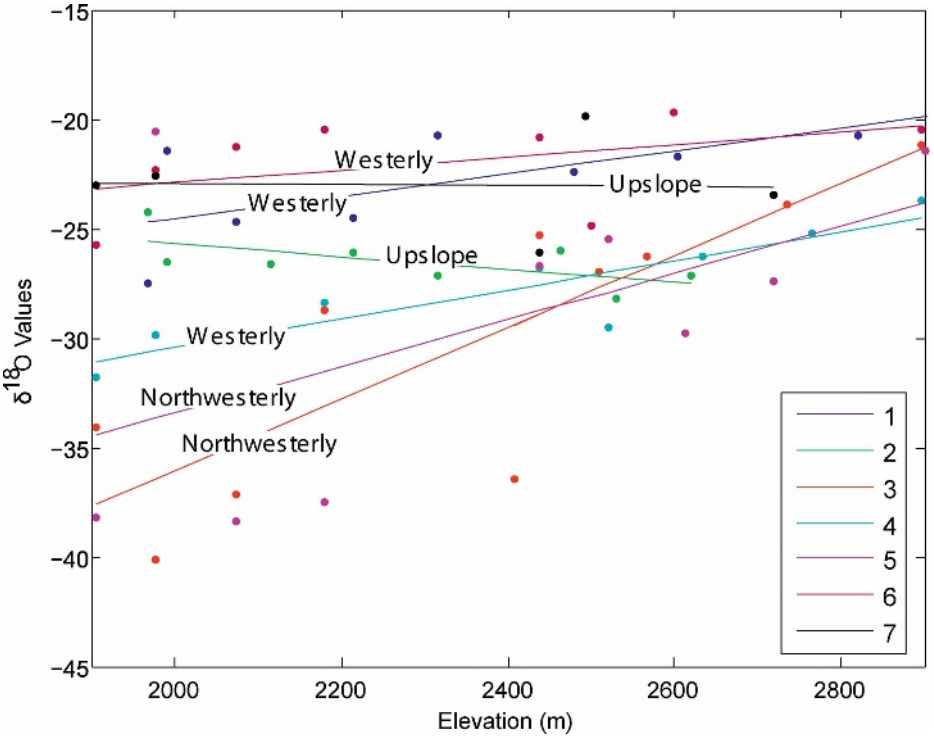

FIGURE 4. $\delta^{18}O$-elevation gradients of the seven snow accumulation events.

TABLE 5

Meteorological conditions and isotopic characteristics of the seven storm events.

	Westerly			Upslope		Northwesterly	
Snowfall Event	1	4	6	2	7	3	5
Isotope data							
Mean $\delta^{18}O$ (‰)	−22.6	−27.7	−22.0	−26.5	−23.0	−30.0	−29.5
$d\delta^{18}O/dz$ (‰/100 m)	0.5	0.7	0.3	−0.3	−0.02	1.6	1.8
NCEP 500 mb flow †							
westerly (m/s)	23.6	20.6	24.6	12.1	7.6	10.8	16.0
northerly (m/s)	0.6	2.5	4.3	−0.9	3.8	7.6	0.9
speed (m/s)	23.6	20.8	25.0	12.2	8.5	13.2	16.1
Specific humidity, q†							
g/kg (850,750 mb)	2.23	2.37	1.95	1.29	2.08	2.56	0.47
anomaly (%)	+15.4	+4.9	+8.6	−42.6	−10.1	−5.1	−73.6
$dq/d\lambda$ (10^6 g/kg m^{-1})	−0.99	−0.71	−0.73	−0.29	+0.20	−0.45	+0.004
start of storm (g/kg)	2.53	2.47	3.18	1.28	2.78	3.54	1.37
end of storm (g/kg)	1.94	2.28	1.67	1.31	2.18	1.23	0.24
Δq during storm (%)	−23.3	−7.7	−47.4	+2.3	−21.6	−65.3	−82.5
Regional snowfall (cm)							
Haig Glacier (2674 m)	11.0	40.0	56.0	32.0	55.0	20.0	4.0
Calgary (1084 m)	1.0	1.6	22.2	7.6	5.8	17.0	5.0
Pocaterra (1610 m)	4.0	17.0	44.0	8.5	9.3	20.0	2.0
Golden, B.C. (785 m)	1.8	9.2	58.0	0.6	2.2	19.2*	1.2
Regional T (°C)							
Haig Glacier	−10.1	−8.8	−13.6	−14.1	−11.1	−12.6	−25.3
Calgary	+1.0	−2.5	−22.0	−11.6	−4.9	−4.6	−19.5
Pocaterra	−3.0	−1.5	−15.3	−9.7	−4.8	−5.3	−21.5
Golden, B.C.	−1.4	−0.7	−9.4	−0.7	−0.9	+1.2	−16.3
Haig Glacier ΔT (C°)‡	−5.1	−5.9	−10.3	−18.5	−10.8	−22.0	−15.3

† Calculated from average daily NCEP fields at the point (51.25°N, 115°W).

* Millimeters of rainfall.

‡ Calculated from the difference in temperature at 00:00 on the first and last day of the snowfall.

which separates B.C. from Alberta. This repeated orographic forcing causes Pacific air masses to lose most of their precipitation in B.C. and on the western slopes of the Canadian Rockies, creating a strong precipitation shadow east of the Continental Divide. Average annual precipitation (rain and snow water equivalent) measured from 2001–2005 at the Haig Glacier AWS (2674 m altitude and a distance of 800 m from the Continental Divide), was 2200 mm, compared with 404 mm in Calgary (Environment Canada, 2006). This precipitation gradient is even higher in the winter months (December, January, February): 430 vs. 27.3 mm water equivalent for winters 2000–2001 to 2004–2005.

Figure 5 depicts the 500 mb geopotential height field and westerly wind anomaly over western Canada for January 27–29, 2004, during storm event 6. This was a large snow accumulation event over the entire region, with 56 cm in Golden, B.C., 55 cm on the Haig Glacier, and 22 cm in Calgary. Storms 1 and 4 also fell under the westerly storm classification and though there was more moisture advection in storm event 6 than in the other two westerly systems, the three events share several common characteristics. These include significant snowfall on westerly slopes and the Continental Divide, and decreasing snow accumulation to the east. These systems were also characterized by moderate temperatures at the Haig and Robertson Glacier sites, with modest cooling (average $\Delta T = -7.3$ C°) over the course of each snowfall event. There was strong 500 mb westerly flow and anomalously strong overall 500 mb flow in each case, accompanied by high 850 and 700 mb vapor mixing ratios, both in the NCEP reanalyses over the region and in the 700 mb sonde data from Kelowna International Airport upstream of the study site. In addition, the air masses experienced significant drying along their eastward trajectory (large negative mixing ratio gradients with longitude, $dq/d\lambda$, over the site).

Under strong westerly flow, precipitation on the westerly slopes of the Canadian Rockies and on the Continental Divide is common despite warm and dry conditions further east. Storm events 1 and 4 were anomalously warm days on the eastern slopes, with strong Chinook conditions evident in Calgary and the foothills region during event 1. Temperatures at the Haig Glacier (Continental Divide) site were 11.1 C° cooler than Calgary during this event. In contrast, event 6 was characterized by temperatures 8.4 C° warmer on the Haig Glacier. This indicates the role of westerly heat and moisture advection at this location; while the lee slopes were under the influence of a cold, shallow continental (cP) air mass during event 6, the higher altitude sites near the Continental Divide were governed by the Pacific air mass. This behavior is typical of winter temperature conditions at the Continental Divide/Robertson Valley sites under strong westerly flow, with the Haig and Robertson Glaciers having a climatological affinity with B.C. rather than the eastern slopes of Alberta. However, this effect can sometimes be masked by adiabatic warming of descending air (Chinook conditions), as witnessed in event 1.

The $\delta^{18}O$-elevation gradients resulting from westerly storms were inverse and positive (i.e., increasing isotopic values with increasing elevation), with values ranging from 0.3‰/100 m to 0.7‰/100 m. $\delta^{18}O$ values were moderate (mean of −24.1‰). This

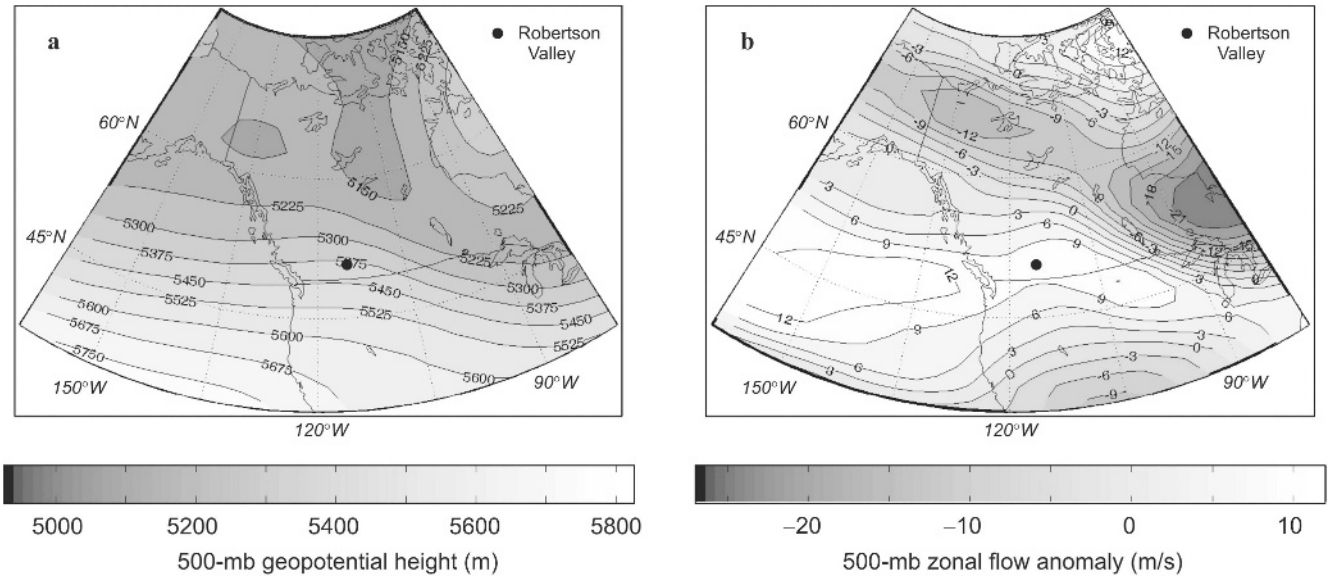

FIGURE 5. NCEP 500-mb (a) geopotential heights (m), and (b) westerly wind anomalies (m/s) in northwestern North America during storm event 6, which is typical of westerly systems that impact the study region. Plots are generated from average daily NCEP Reanalyses from January 27–29, 2004. The zonal wind anomaly is based on monthly mean (January) zonal wind fields for the period 1948–2005.

data is consistent with continuous Rayleigh distillation as air masses flow over the Continental Divide and continue to precipitate. In the Robertson Valley, snow deposited by these systems could include advected hydrometeors that condense upstream of the Divide, or the snow may consist of moisture that condenses locally as westerly air masses mix with cooler air on the lee side of the Divide.

Upslope Storm Systems

Easterly, upslope flow is regional in scale and is common in all seasons in the eastern slopes of the Canadian Rockies. In spring, summer, and autumn, upslope flow is associated with the passage of extratropical cyclones south of the study area, which can bring heavy orographic precipitation to the region. We did not sample any of these systems. In winter months, upslope flow is most commonly associated with cold, dry continental air masses that move south from the Canadian Arctic, creating a surface high east of the Rockies. These high pressure systems drive air masses up the eastern slopes of the Rockies, turning them to windward precipitation slopes. Total precipitation from these systems typically increases with altitude and distance upslope as air masses are lifted by the combined influence of orography and the incoming cold front.

Figure 6 depicts the 500 mb height field and flow strength anomalies from storm event 2, which we have categorized as an upslope system. Event 7 also fell into this classification. The upper-air synoptic pattern in Figure 6 is typical of winter upslope

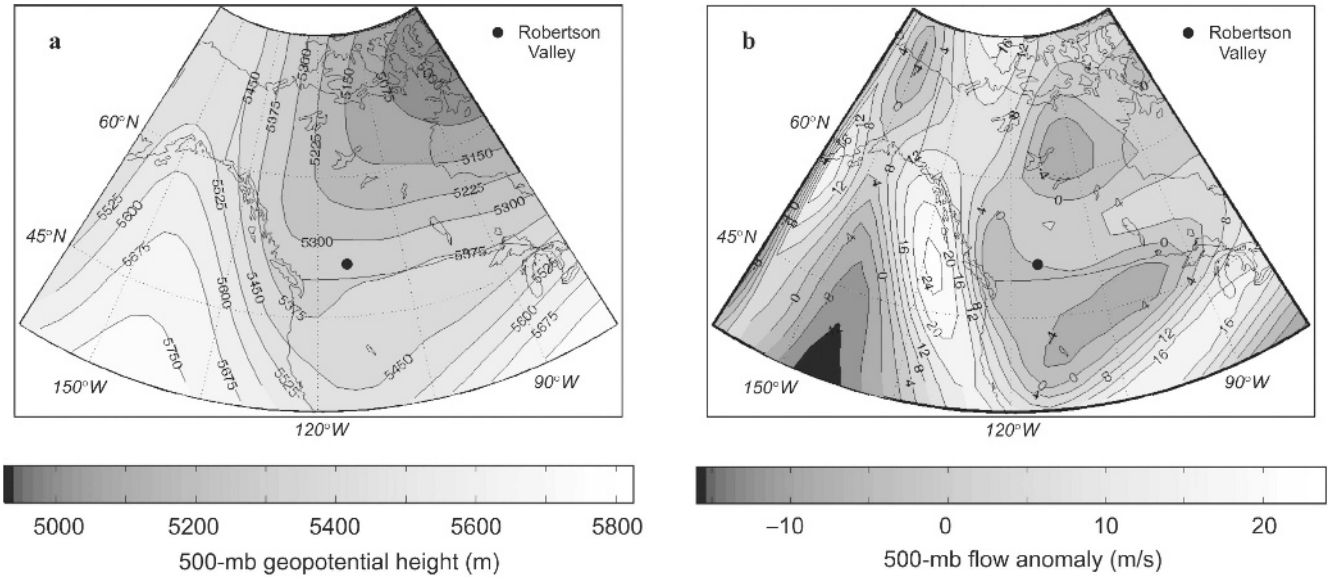

FIGURE 6. NCEP 500-mb (a) geopotential heights (m), and (b) geostrophic wind anomalies (m/s) in northwestern North America during storm event 2, which is typical of upslope systems that impact the study region. Plots are generated from average daily NCEP Reanalyses from March 15–16, 2002. The geostrophic wind anomaly is based on mean March flow for the period 1948–2005.

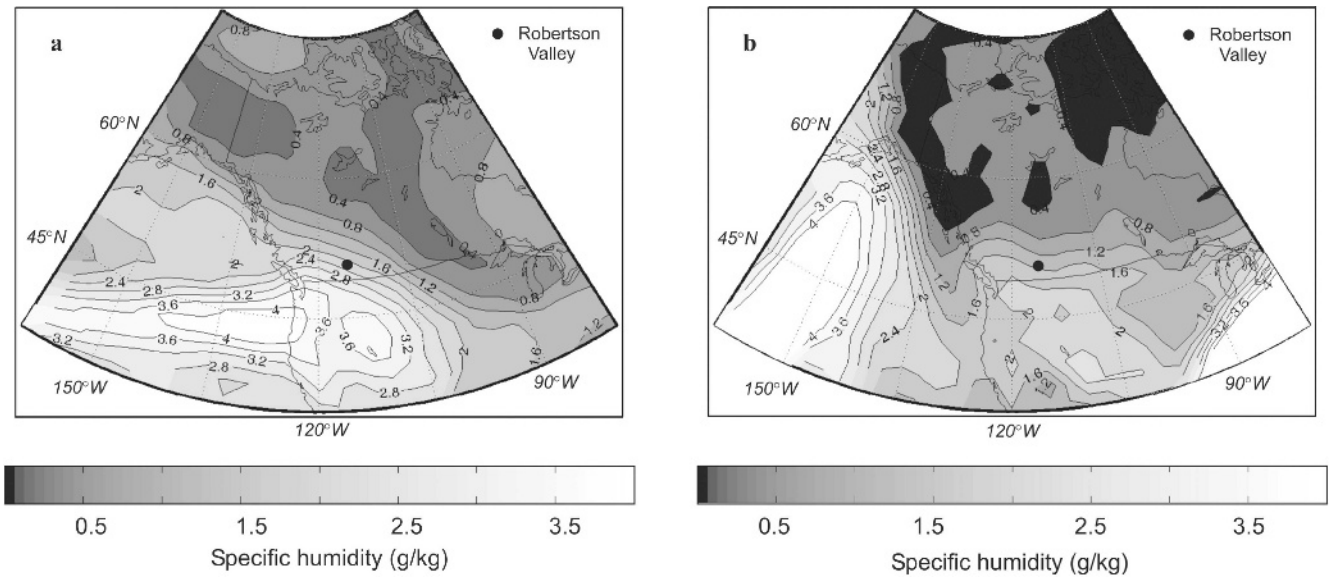

FIGURE 7. Lower troposphere specific humidity (g/kg) in northwestern North America during storm events (a) 6 (westerly), and (b) 2 (upslope), as plotted in Figures 5 and 6, respectively. Plots are generated from daily NCEP Reanalyses for January 27–29, 2004, and March 15–16, 2002, averaged for 850 and 700 mb. Scale bars are identical and contour intervals are 0.4 g/kg.

systems, with an upper-level trough over western Canada and ridging in the North Pacific. When strong enough, this pattern effectively blocks zonal heat and moisture transport to the study site, with weak upper-level flow in the region and strong northerly storm tracks well west of the Continental Divide. Storm events 2 and 7 were characterized by weak 500 mb westerly and total flow.

As seen in Table 5, events 2 and 7 were characterized by high snow accumulation on the Haig Glacier relative to all other sites: three to 10 times the snow accumulation measured at lower altitude sites on the eastern slopes. There was little or no snow accumulation on western slopes of the Rockies. Large temperature decreases were measured during the snow accumulation event on the Haig Glacier (an average cooling of 14.7 C°), which was consistently cooler than all other sites. Relatively weak surface temperature lapse rates prevailed in the eastern slopes during these events (~ -3 C° km^{-1}), typical of mean winter lapse rates in the region (Shea et al., 2004). There was a marked decoupling of temperature patterns across the Divide, with Golden anomalously warm relative to the eastern slopes. In contrast to strong westerly systems, however, temperatures at the Haig and Robertson Glaciers covaried with eastern rather than western sites during these events.

Lower troposphere specific humidity was low in the study region in both of these events. There was also an unusual occurrence of greater atmospheric moisture east of the Continental Divide during event 7 ($dq/d\lambda = +0.2 \times 10^6$ g/kg m^{-1}). To illustrate the fundamental differences in atmospheric moisture patterns in westerly vs. upslope systems, Figure 7 plots specific humidity over northwestern North America for snow accumulation events 6 (westerly) and 2 (upslope). These maps are based on the average 850 and 700 mb moisture for the same dates as the 500 mb patterns of Figures 5 and 6. These atmospheric levels are considered representative of moisture advection sources at the altitude of the Canadian Rockies. Figure 7a depicts the moisture advection that is typical under westerly flow, as well as the strong eastward depletion of moisture in the study area. Figure 7b is representative of upslope systems, with drier air masses prevailing over western Canada and blocking/southward diversion of Pacific moisture sources clearly evident in this image.

Altitudinal gradients of $\delta^{18}O$ in these systems were negative (similar to classical windward slopes), with values of −0.02‰/100 m to −0.3‰/100 m.

Northwesterly Storm Systems

The third type of synoptic setup, which we call northwesterly flow, is a complex hybrid of the westerly and upslope synoptic patterns. Westerly flow still penetrates the Continental Divide but is weakened and dried from the influence of cP air descending over western Canada, diverting storm tracks southward and bringing significant precipitation to the western slopes as air is cooled across southern B.C. The main contrast with upslope storms, which also involve upper-level troughs (cP air masses moving southward into the region), is that there is effective blocking of westerly flow in upslope storms, with negligible precipitation on the western slopes of the Rockies. In the case of northwesterly flows, there is weak/incomplete blocking, and Pacific moisture still penetrates to the Continental Divide and eastern slopes of the Rockies.

Figure 8a depicts NCEP 500 mb patterns in northwestern North America for storm event 3, which we have categorized as a northwesterly system at our site. Storm event 5 was also classified as northwesterly, despite the very different temperature and snow accumulation totals in the two events. Westerly and total 500 mb flow were weak in each event but stronger than the upslope storm configuration. Ridging in the North Pacific is similar to the 500 mb pattern for upslope systems, with strong northerly flow in western Canada diverting lower troposphere moisture to the south of the study area. Unlike the upslope case, high levels of moisture are still ushered into the region from the west. Storms 3 and 5 were both characterized by widespread precipitation, with similar precipitation totals west, east, and atop the Continental Divide.

Temperature plunged over the course of each storm, with anomalously cold conditions at the end of each snowfall event: −18.5 C° below the monthly normals in Calgary. There was an average cooling of −18.7 C° on the Haig Glacier over the two events. These storms developed into more classical upslope systems after the snow accumulation on the Haig and Robertson

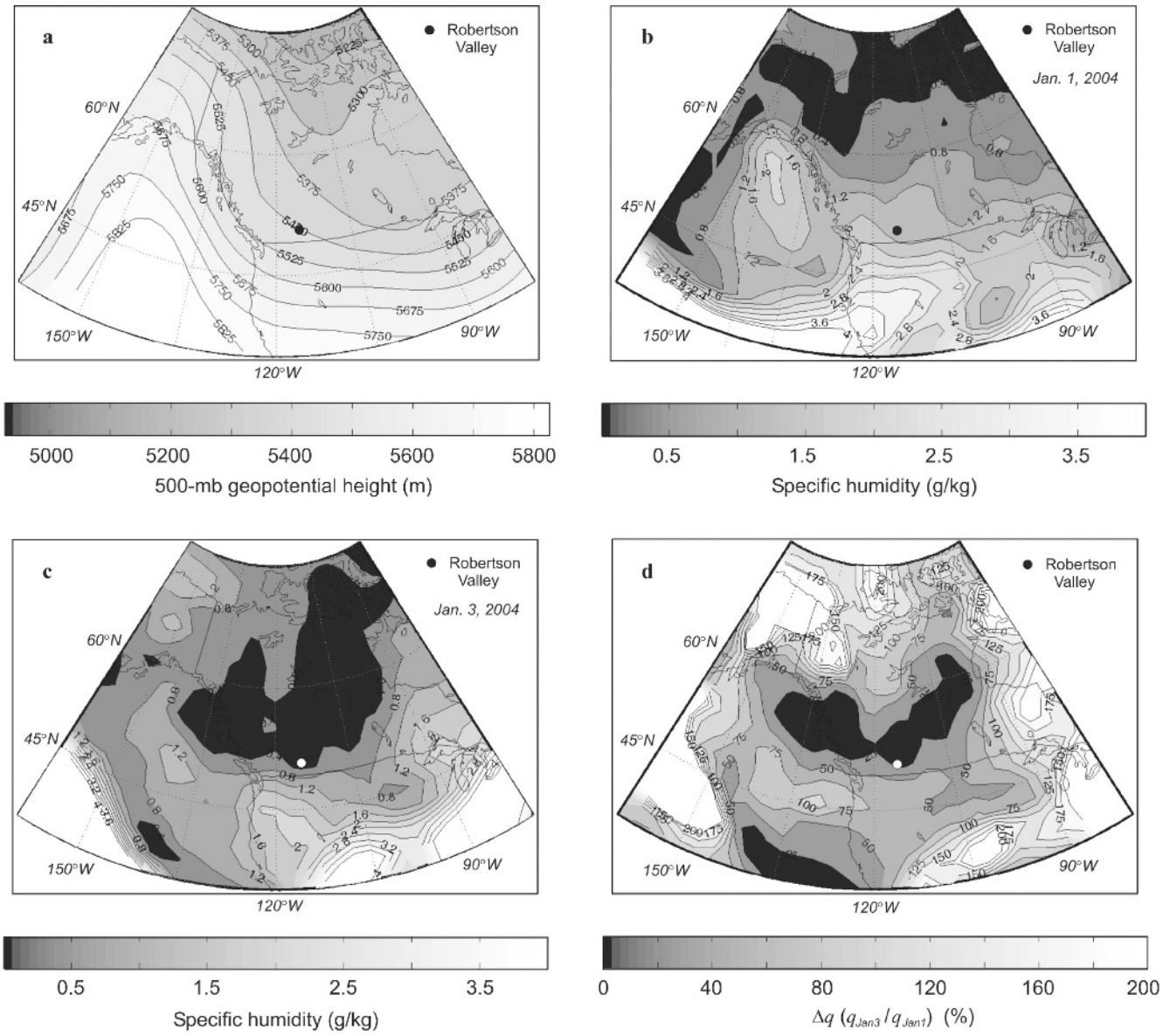

FIGURE 8. NCEP geopotential height and specific humidity patterns in northwesterly snow accumulation events. (a) 500-mb geopotential height in storm event 3, October 28–30, 2003 (m). (b) and (c) Lower troposphere specific humidity in northwestern North America during storm event 5 (g/kg): (b) January 1, 2004, the start of the snowfall event, and (c) January 3, 2004, the end of the snowfall event. (d) Change in specific humidity over this snowfall event, 100 × (q_{Jan3}/q_{Jan1}) (%). Plots are averaged from daily average 850 and 700 mb levels in the atmosphere.

Glaciers, as the upper-level trough strengthened and expanded to the south and west. Calgary continued to receive snowfall during the passage of the trough (from October 31, 2003 to November 4, 2003), but no further snowfall was recorded at the Continental Divide site after October 29, 2003. Golden, B.C., received 19.2 mm of rain during this event, all on October 28, 2003. We appear to have experienced a transition from westerly to upslope conditions, with snow accumulation at the Continental Divide sites governed by the first phase of the progression.

Specific humidity levels differed markedly in storms 3 and 5, in part because the first took place in October and the latter event occurred in January, when a cold, continental air mass was well established in the region. The cP air masses force the polar jet stream south, causing subsidence and drying of the air mass on the western side of the Canadian Rockies. This effect is seen in the sonde data from Kelowna, B.C., where strong drying of the lower troposphere was observed from the start to the end of events 3 and 5. Northwesterly flow escorts dry northern air masses into southern B.C. and Alberta, leading to general depletion of water vapor in the lower troposphere. This is seen throughout southwestern B.C. and Alberta, as indicated by the change in specific humidity over the Robertson Valley site (Table 5)—reductions of 65.3% and 82.5% for storms 3 and 5, the greatest drying out of the seven snow systems that we sampled. This is consistent with the severe cooling over the course of these two snow events.

Despite the large differences in snowfall between events 3 and 5, $\delta^{18}O$ values and altitudinal gradients were similar and were relatively extreme. Isotopic ratios near −40‰ were measured from the base of the Robertson Valley, and both systems were characterized by steep, inverse isotopic-altitude gradients: +1.6‰/100 m and +1.8‰/100 m.

Discussion

Air mass trajectory played a key role in determining the $\delta^{18}O$-elevation gradient of precipitation in the Robertson Valley. Both westerly and easterly (upslope) weather systems contribute to snow accumulation at the site, with substantial snowfall possible in each case. The valley is a lee-slope setting for westerly systems, but is close enough to the Continental Divide to receive a large amount of precipitation under these synoptic conditions. This precipitation could originate from orographically cooled air masses on the windward slopes, with snow swept over the Divide by strong winds that characterize the site, or through continued cooling and condensation of vapor as air masses cross the Divide and mix with cooler air in the lee slopes.

Either of these precipitation mechanisms is consistent with the inverse isotope-altitude gradients that we measured at the site. Continued Rayleigh distillation of air masses leads to increasing ^{18}O-depletion (more negative $\delta^{18}O$) at lower altitudes, in proportion to distance from the Divide. The two upslope snowfall events that we sampled had the opposite relationship, with a more conventional decrease in $\delta^{18}O$ with altitude.

Only seven snow events were sampled, precluding meaningful statistical analysis of our results. From this limited data, there is a weak but positive correlation between local temperature (Haig and Robertson Glaciers) and mean $\delta^{18}O$ in each snowfall event ($r = 0.44$). This implies that over 80% of the variance in the data is associated with influences other than the local condensation temperature. Differences in the average $\delta^{18}O$ and the $\delta^{18}O$-elevation gradient in each snow event most likely reflect the position of the vapor mass on the Rayleigh distillation curve (cf. Fig. 1). This, in turn, is a function of the vapor source region, the air mass trajectory through western North America, and the amount of rainout along this trajectory. For westerly and northwesterly systems, most of the rainout from the air mass takes place on the windward slopes, giving rise to potentially large isotopic gradients in the late stages of air-mass drying over a scale of just a few kilometers in the lee of the Divide. Strong westerly systems that brought precipitation to the region were characterized by rapidly diminishing snow accumulation east of the Divide, consistent with this interpretation. In addition, $\delta^{18}O$-elevation gradients are correlated with mean $\delta^{18}O$ for the seven events ($r = -0.71$), indicating tight coupling of $\delta^{18}O$ values and their rate of change, consistent with Rayleigh distillation (Fig. 1). More snowfall events would need to be sampled to explore this further.

Northwesterly snow accumulation systems are somewhat enigmatic. These systems exhibited the largest isotopic depletion downstream of the Divide and the most negative $\delta^{18}O$ values that we have recorded in several years of snow-isotope work in the region. Following the reasoning above, this should indicate extreme late-stage Rayleigh distillation. This is not definitive in the snow accumulation totals, as eastern slope sites received as much or more snow as the Haig and Robertson Glaciers in northwesterly events 3 and 5. However, the severe drying of the air masses in the region over the course of these two events (Table 5) does imply late-stage Rayleigh distillation. Figures 8b–8d illustrate the severe drying throughout western Canada from January 1 to January 3, 2004, during snow event 5. The entire study region loses over 75% of its lower tropospheric moisture over this 48 hour period. This is also seen in the radiosonde data from Kelowna, B.C.

The severe aridification of the air masses in these two events is consistent with late-stage Rayleigh distillation as a plausible explanation of the light isotopic ratios and the large gradient in $\delta^{18}O$ downslope of the Divide—depletions of 15–18‰ over a distance of several kilometres. The northwesterly trajectory of the air masses would contribute to this effect, as air masses originating in the northeast Pacific would be cooler and less humid than those from lower latitudes. Moreover, air masses originating from the northeast Pacific experience a greater distance of overland travel, with cooler surface temperatures and more orographic forcing than direct westerly flows. These effects promote greater fractional rainout during air-mass transit to the study site.

Storms of short duration (three days or less) with a single identifiable moisture source were more likely to have a significant $\delta^{18}O$-elevation gradient than storm systems of longer duration (four or more days). Long-duration storms may have experienced moisture from more than one source region and they produced precipitation under a large range of condensation temperatures over the course of the storm. Snow accumulation events 6 and 7 were both comprised of more than one storm type and were of long duration (9–10 days), but were classified as westerly and upslope storms, respectively, based on the dominant weather pattern at the time of snow accumulation in the region. Our field sampling procedure may also have led to mixing of precipitation from different days during each event, leading to the greater scatter in the $\delta^{18}O$ values and the lack of a statistically significant $\delta^{18}O$-elevation gradient in the regression vs. altitude.

COMPARISON WITH SNOW-WATER ISOTOPES IN CALGARY, ALBERTA

The inverse $\delta^{18}O$-elevation gradients that we measure appear more prevalent in the Robertson Valley than the conventional ^{18}O depletion with altitude. This is supported by integrated winter snowpack data that is available from the Haig Glacier site vs. $\delta^{18}O$ in Calgary snowfall. End-of-winter snowpits were sampled on the Haig Glacier in 2002, 2004, and 2005, with density-weighted mean $\delta^{18}O$ values of −21.3‰, −18.5‰, and −19.5‰. Unfortunately, snow-isotope data is unavailable for Calgary, Alberta, for these years, but the amount-weighted 10-year mean value in Calgary for winter (December, January, February) 1992–2001 was -26.3 ± 1.9‰ (calculated from Table 1 of Peng et al., 2004). This implies that the altitudinal inversion is a persistent feature of the eastern slopes, and that the westerly and northwesterly storms that we have sampled dominate the winter snowpack on the eastern slopes of the Canadian Rockies.

MODELING RAYLEIGH DISTILLATION GRADIENTS

We have hypothesized that $\delta^{18}O$-elevation gradients at our site can be explained as late-stage rainout in a simple single-stage Rayleigh distillation as air masses cross the Continental Divide. However, Rayleigh distillation is non-linear (Fig. 1), whereas we have presented linear altitudinal gradients for the seven snowfall events. This was done to permit comparison with the linear $\delta^{18}O$-altitude gradients that are reported from the majority of published studies. Our field data is also derived from a small portion of the Raleigh curve—an air mass trajectory of approximately 10 km, relative to a distance of ~ 600 km from Pacific moisture sources. We have assumed that the $\delta^{18}O$ depletion can be approximated as linear along this small portion of the distillation curve. Statistically significant results were also found for quadratic regressions but at a lower significance. Though we assume that a linear relationship is a reasonable approximation for local $\delta^{18}O$ gradients, a non-linear relationship would be expected for $\delta^{18}O$ gradients over a larger spatial scale such as the entire distillation path from the Pacific Ocean to the Canadian Rockies.

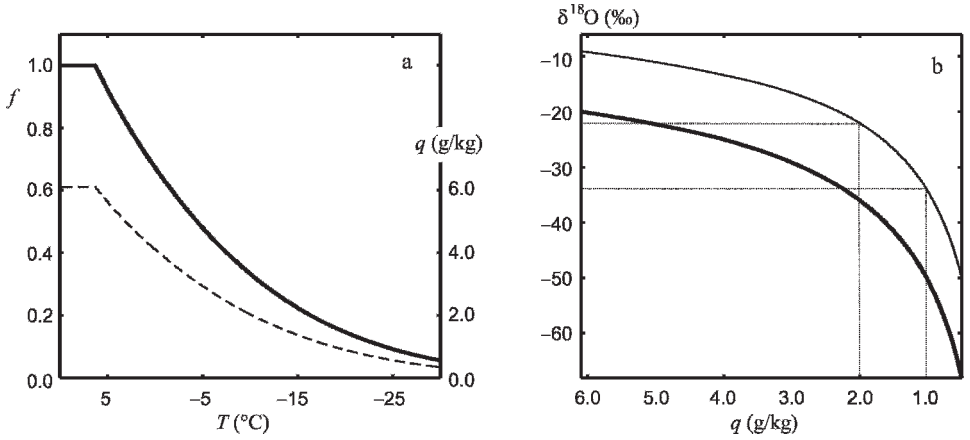

FIGURE 9. Rayleigh distillation of ^{18}O in a simple scenario where the air mass cools from 10°C to −30°C through mixed isobaric/orographic cooling. We assume equilibrium condensation of a mixture of ice crystals and supercooled droplets, with distinct, temperature-dependent fractionation coefficients for ice and liquid. (a) Evolution of air mass vapor fraction f (solid line) and specific humidity q (dashed line) as a function of temperature, from 10°C to −30°C. (b) $\delta^{18}O$ of vapor (heavy line) and condensate (thin line) as a function of specific humidity q.

We explore this in a simple model for the entire air mass trajectory from the Pacific source region. Building on the classical Rayleigh distillation that was illustrated in Figure 1 (Equations 1–3), we construct a physically plausible scenario for our study region. The residual vapor fraction in the cloud, f, can be couched in terms of the specific humidity through $f = q/q_0$, where q_0 is the initial specific humidity in the air mass. Specific humidity is related to vapor pressure, e_v, through

$$q = \frac{Re_v}{R_v P} \approx 0.622\frac{e_v}{P}, \tag{4}$$

where R and R_v are the ideal gas law constants for the bulk air mass and for pure vapor and P is the total pressure (e.g., Bohren and Albrecht, 1998: 186).

We assume a scenario in which a Pacific air mass begins at 10°C and a relative humidity of 80%, which are typical of winter conditions in the region. The air mass travels eastward to the continental interior and is assumed to cool to −30°C along its trajectory through a combination of isobaric and orographic cooling. We also assume that the air mass remains saturated once it cools to its dew point, allowing vapor pressure to be calculated as a function of temperature. These conditions correspond with a mixed cloud that includes a mixture of vapor, ice crystals, and supercooled liquid droplets from 0°C to −30°C. The saturation vapor pressure over liquid water and ice are calculated from the Clausius-Clapeyron equation,

$$\begin{aligned} e_{sl} &= 6.11\exp\left[6808\left(\frac{1}{T_0} - \frac{1}{T}\right) - 5.09\ln\left(\frac{T}{T_0}\right)\right]; \\ e_{si} &= 6.11\exp\left[6293\left(\frac{1}{T_0} - \frac{1}{T}\right) - 0.555\ln\left(\frac{T}{T_0}\right)\right], \end{aligned} \tag{5}$$

where $T_0 = 273.15$ K (Bohren and Albrechts, 1998: 198–199). We prescribe a simple mixture of ice crystals and supercooled water droplets in our scenario, with 100% liquid droplets at 0°C and 100% ice crystals at −30°C, and an ice fraction θ that varies linearly between these two end members. The effective vapor pressure of the air mass can then be approximated by

$$e_v(T) = \theta(T)\, e_{si}(T) + [1 - \theta(T)]\, e_{sl}(T). \tag{6}$$

For isobaric cooling, the vapor reservoir fraction f can be calculated as a direct function of temperature: $f = q/q_0 = e_v/e_{v0}$. In the more realistic case where cooling of the air mass occurs through a combination of isobaric cooling (e.g., through continental effects) and orographic uplift, pressure decreases with altitude and this effect needs to be included in the estimation of f. For the illustrative scenario here, we prescribe a pressure decrease from 1000 to 700 mb, concomitant with the cooling from 10°C to −30°C, reflecting the net orographic forcing for lower tropospheric air masses traversing southwestern Canada.

Figure 9 plots the evolution of f, q, $\delta^{18}O_v$, and $\delta^{18}O_p$ for Rayleigh distillation in the case with mixed isobaric/orographic cooling. The air cools to 6.3°C before it saturates, with $f = 1$ and $q = q_0 = 6.1$ g/kg until that point. Cooling to −30°C and uplift to 700 mb leave a residual vapor fraction $f = 0.06$ and a specific humidity $q = 0.24$ g/kg at the end of the air mass trajectory. An initial cloud vapor isotopic ratio $\delta^{18}O_{v0} = -20‰$ is adopted in Figure 9b. This gives initial rainout with a value of $\delta^{18}O_p \approx -10‰$, consistent with typical winter precipitation from mid-latitude Pacific air masses in Victoria, B.C. (IAEA/WMO, 2004).

Note that Figure 9b plots the distillation as a function of specific humidity rather than vapor fraction f, permitting more direct comparison with meteorological data or reanalyses (e.g., Fig. 8). Precipitation isotopes and specific humidities in this scenario are typical of those in our study area: $\delta^{18}O_p$ from −22.1‰ to −34.2‰ for specific humidities of 2 to 1 g/kg. The change in $\delta^{18}O_p$ with specific humidity, $d\delta^{18}O_p/dq$, offers a complementary constraint. The drying from $q = 2$ to $q = 1$ g/kg coincides with a 12.1‰ decrease in $\delta^{18}O_p$, for instance. The same absolute change in specific humidity, from $q = 1.5$ to $q = 0.5$ g/kg, corresponds with an isotopic depletion of 23.2‰. This illustrates the strong depletion and large spatial $\delta^{18}O$ gradients that can be expected in late-stage Rayleigh distillation.

We have assumed equilibrium fractionation under condensation, using liquid-vapor fractionation coefficients in Equation 3 and ice-vapor fractionation coefficients from Majoube (1971),

$$1000\ln\left[\alpha(T)_{i-v}\right] = 11839/T - 28.224. \tag{7}$$

In reality, mixed cloud processes will prevail at these temperatures and kinetic fractionation can be expected during the migration of vapor from supercooled water droplets to ice crystals (Jouzel et al., 1984). The Rayleigh distillation plots in Figure 9 are simply illustrative and we do not address this process here. This effect is potentially significant for winter precipitation in the region, and its magnitude needs to be assessed in future work.

Detailed meteorological modeling of the individual snow accumulation events is needed to explore this further. We propose, in particular, that the introduction of isotope transport and fractionation processes in a mesoscale meteorological model

would be fruitful for analysis of different air-mass trajectories and specific storm events in western North America.

As a final note, we have not presented δD data here, but general Rayleigh distillation processes discussed for $\delta^{18}O$ extend equally to hydrogen isotopes. Because ^{18}O and ^{2}H have different fractionation coefficients, they follow a separate path under Rayleigh distillation, which gives rise to different temperature dependencies and $d\delta/df$ gradients. In settings where single-stage Rayleigh distillation is a good approximation, this could also be exploited in a spatial network of precipitation samples to provide additional constraints on air mass evolution and cloud properties (temperature; position on the Rayleigh curve, f).

Conclusions

The eastern slopes of the Canadian Rocky Mountains provide an interesting area in which to study the dynamics of isotopes on lee slopes because vapor masses contributed precipitation to the area from both westerly and upslope storm trajectories, occasionally causing lee slopes to become windward slopes. Storm trajectories are the dominant control on $\delta^{18}O$-elevation gradients in the Robertson Valley, determining both the sign and the magnitude of the $\delta^{18}O$-elevation gradient. From the limited data available at this time, we argue that inverse $\delta^{18}O$-elevation gradients can be qualitatively explained by ongoing Rayleigh distillation as westerly air masses cross the Continental Divide and continue to precipitate. Isotopic depletion with distance from the Divide may offer insight into the position of the vapor mass on the Rayleigh distillation curve. We will pursue this hypothesis in future work to test whether winter precipitation in the region can be effectively modeled as a single-stage Rayleigh distillation process.

Preliminary analysis suggests that average $\delta^{18}O$ values and $\delta^{18}O$-elevation gradients in discrete snow accumulation events can be related to synoptic weather systems and snow accumulation patterns in the region. Further constraints on these relationships may create the possibility of using snow-water isotopes as a new tool to assess the synoptic meteorological controls on wintertime precipitation in the eastern slopes of the Canadian Rockies. For instance, end-of-winter snowpit isotope stratigraphies could be interpreted in terms of the percentage contribution to the snowpack from different weather systems. Since direct meteorological and hydrological observations from alpine sites are sparse in Canada, this would be of value to water resource forecasts and glacier mass-balance studies.

The results also suggest the need for caution in applications of $\delta^{18}O$-elevation gradients in paleoaltimetry and paleoclimate reconstructions. $\delta^{18}O$-elevation gradients in windward slopes can be assumed to be negative, but actual values will depend on latitude and continentality (distance from the moisture source). $\delta^{18}O$-elevation gradients in lee-slope settings are difficult to generalize, but can be expected to be inverse unless there are significant sources of moisture from lee-slope air masses.

Acknowledgments

We thank Andrea McCormick and Brian Horton for their tireless assistance collecting field samples. Steve Taylor of the University of Calgary Stable Isotope Laboratory helped to run the water samples, and Judy Buchanan-Mappin (Kananaskis Field Station) and Rick Smith (University of Calgary Weather Research Station) provided meteorological data. Thoughtful suggestions from two anonymous reviewers have improved the manuscript. Financial support for this research was provided by the Natural Sciences and Engineering Research Council (NSERC), Canada.

References Cited

Ambach, W., Dansgaard, W., Eisner, H., and Møller, J., 1968: The altitude effect on the isotopic composition of precipitation and glacier ice in the Alps. *Tellus*, 20: 595–600.

Banta, R. M., 1990: The role of mountain flows in making clouds. *In* Blumen, W. (ed.), *Atmospheric processes over complex terrain*. Boston: American Meteorological Society, Meteorological Monograph, 23(45): 229–283.

Barnett, T. P., Adam, J. C., and Lettenmaier, D. P., 2005: Potential impacts of warming climate on water availability in snow-dominated regions. *Nature*, 438: 303–309.

Bohren, C. F., and Albrecht, B. A., 1998: *Atmospheric thermodynamics*. Oxford, New York: Oxford University Press, 186–199.

Bowen, G. J., and Wilkinson, B., 2002: Spatial distribution of $\delta^{18}O$ in meteoric precipitation. *Geology*, 30(4): 315–318, doi:10.1130/0091-7613.

Byrne, J. M., Berg, A., and Townshend, I., 1999: Linking observed and general circulation model upper air circulation patterns to current and future snow runoff from the Rocky Mountains. *Water Resources Research*, 35: 3793–3802.

Chamberlain, C. P., and Poage, M. A., 2000: Reconstructing the paleotopography of mountain belts from the isotopic composition of authigenic minerals. *Geology*, 28: 115–118.

Chung, Y. S., Hage, K. D., and Reinelt, E. R., 1976: On lee cyclogenesis and airflow in the Canadian Rocky Mountains and East Asian Mountains. *Monthly Weather Review*, 104: 879–891.

Craig, H., 1961: Isotopic variations in meteoric waters. *Science*, 133(3464): 1702–1703.

Dansgaard, W., 1964: Stable isotopes in precipitation. *Tellus*, 16: 436–468.

Dansgaard, W., Johnsen, S. J., Clausen, H. B., and Gundestrup, N., 1973: Stable isotope glaciology. *Meddeleelser om Grönland*, 197: 1–53.

Dettman, D. L., and Lohmann, K. C., 2000: Oxygen isotope evidence for high altitude snow in the Laramide Rocky Mountains of North America during the Late Cretaceous and Paleogene. *Geology*, 28(3): 243–246, doi: 10.1130/0091-7613.

Drummond, C. N., Wilkinson, B. H., Lohmann, K. C., and Smith, G. R., 1993: Effect of regional topography and hydrology on the lacustrine isotopic record of Miocene paleoclimate in the Rocky Mountains. *Paleogeography, Paleoclimatology, Paleoecology*, 101: 67–79.

Environment Canada, 2006: Canadian Climate Data. (http://www.climate.weatheroffice.ec.gc.ca/climateData/canada_e.html). Last accessed on June 12, 2007.

Friedman, I., and Smith, G. I., 1970: Deuterium content of snow cores from Sierra Nevada area. *Science*, 169: 467–470.

Garizone, C. N., Quade, J., DeCelles, P. G., and English, N. B., 2000: Predicting the paleoelevation of Tibet and the Himalaya from $\delta^{18}O$ vs. altitude gradients in meteoric water across the Nepal Himalaya. *Earth and Planetary Science Letters*, 183: 215–229.

Gat, J. R., 1980: The isotopes of hydrogen and oxygen in precipitation. *In* Fritz, P., and Fontes, J.-Ch. (eds.), *Handbook of environmental isotope geochemistry, vol. 1, the terrestrial environment*. Amsterdam: A. Elsevier, 21–48.

Gat, J. R., Mook, W. G., and Meijer, H. A. J., 2000: Atmospheric water. *In* Mook, W. G. (ed.), *Environmental isotopes in the hydrological cycle: principles and applications, volume II, atmospheric water*. Vienna: International Atomic Energy Agency, 117 pp.

Grasby, S. E., and Lepitzki, D. A. W., 2002: Physical and chemical properties of the Sulphur Mountain thermal springs, Banff National Park, and implications for endangered snails. *Canadian Journal of Earth Sciences*, 39: 1349–1361.

Holdsworth, G., Fogarasi, S., and Krouse, H. R., 1991: Variation of the stable isotopes with altitude in the Saint Elias Mountains of Canada. *Journal of Geophysical Research*, 96: 7483–7494.

Horita, J., and Wesolowski, D. J., 1994: Liquid-vapour fractionation of oxygen and hydrogen isotopes of water from freezing to the critical temperature. *Geomchimica et Comsmochimica Acta*, 58: 3425–3437.

IAEA/WMO, 2004: Global Network of Isotopes in Precipitation. GNIP Database (http://isohis.iaea.org). Last accessed on June 12, 2007.Jouzel, J., Merlivat, L., and Lorius, C., 1984: Deuterium and oxygen-18 in precipitation: modeling the isotopic effects during snow formation. *Journal of Geophysical Research*, 89(D7): 11,749–11,757.

Lapp, S., Bryne, J., Kienzle, S., and Townshend, I., 2002: Linking global circulation model synoptics and precipitation for western North America. *International Journal of Climatology*, 22: 1807–1817.

Lorius, C., and Merlivat, L., 1975: Distribution of mean surface stable isotope values in East Antarctica: observed changes with depth in the coastal area. *International Association of Hydrological Sciences Publication*, 118: 127–137.

Majoube, M., 1971: Fractionnement en oxygène-18 et en deutérium entre l'eau et sa vapeur. *Journal of Chemical Physics*, 197: 1423–1436.

Merlivat, L., and Nief, G., 1967: Isotopic fractionation of solid-vapour and liquid-vapour changes of state of water at temperatures below 0°C. *Tellus*, 19: 122–127.

Moser, H., and Stichler, W., 1974: Deuterium and oxygen-18 contents as an index of the properties of snow covers. *International Association of Hydrological Sciences Publication*, 114: 122–135.

Niewodniczański, J., Grabczak, J., Barański, L., and Rzepka, J., 1981: The altitude effect on the isotopic composition of snow in high mountains. *Journal of Glaciology*, 27: 99–111.

Peng, H., Mayer, B., Harris, S., and Krouse, H. R., 2004: A 10-year record of stable isotope compositions of hydrogen and oxygen in precipitation at Calgary, Alberta, Canada. *Tellus* B, 56(2): 147–159.

Pierrehumbert, R. T., 1999: Huascaran $\delta^{18}O$ as an indicator of tropical climate during the Last Glacial Maximum. *Geophysical Research Letters*, 26(9): 1345–1348.

Poage, M. A., and Chamberlain, C. P., 2001: Empirical relationships between elevation and the stable isotope composition of precipitation and surface waters: considerations for studies of paleoelevation change. *American Journal of Science*, 31: 1–15.

Roe, G. H., 2005: Orographic precipitation. *Annual Reviews of Earth and Planetary Sciences*, 33: 645–671.

Rood, S. B., Samuelson, G. M., Weber, K. A., and Wyrot, K. A., 2005: Twentieth-century decline in streamflows from the hydrographic apex of North America. *Journal of Hydrology*, 306: 215–233.

Rowley, D. B., and Currie, B. S., 2006: Palaeo-altimetry of the late Eocene to Miocene Lunpola basin, central Tibet. *Nature*, 439: 677–681.

Rowley, D. B., Pierrehumbert, R. T., and Currie, B. S., 2001: A new approach to stable isotope-based paleoaltimetry: implications for paleoaltimetry and paleohypsometry of the high Himalaya since the Late Miocene. *Earth and Planetary Science Letters*, 188: 253–268.

Różański, K., Araguás-Araguás, L., and Gonfiantini, R., 1993: Isotopic patterns in modern global precipitation. *In* Swart, P. K., Lohwan, K. L., McKenzie, J., and Savin, S. (eds.), *Climatic change in continental isotopic records*. Washington: American Geophysical Union, Geophysical Monograph, 78: 1–36.

Shea, J. M., Marshall, S. J., and Livingston, J. L., 2004: Climate controls on glacier distribution in the Canadian Rockies. *Arctic, Antarctic, and Alpine Research*, 36(2): 272–280.

Stewart, R. E., Bachand, D., Dunkley, R. R., Giles, A. C., Lawson, B., Legal, L., Miller, S. T., Murphy, B. P., Parker, M. N., Paruk, B. J., and Yau, M. K., 1995: Winter storms over Canada. *Atmosphere-Ocean*, 33(2): 233–247.